Stress analysis of double-lap bi-material joints bonded with thick adhesive

Saleh, Mohamed Nasr; Saeedifar, Milad; Zarouchas, Dimitrios; Freitas, Sofia Teixeira De

DOI
10.1016/j.ijadhadh.2019.102480

Publication date
2020

Document Version
Final published version

Published in
International Journal of Adhesion and Adhesives

International Journal of Adhesion & Adhesives 97 (2020) 102480

Contents lists available at ScienceDirect

International Journal of Adhesion and Adhesives

journal homepage: http://www.elsevier.com/locate/ijadhadh

Stress analysis of double-lap bi-material joints bonded with thick adhesive

Mohamed Nasr Saleh *, Milad Saeedifar, Dimitrios Zarouchas, Sofia Teixeira De Freitas

Structural Integrity & Composites, Faculty of Aerospace Engineering, Delft University of Technology, Delft, 2629 HS, the Netherlands

ARTICLE INFO

Keywords:
Metals
Composites
Stress analysis
Mechanical properties of adhesives
Shear-lag model
AE
Acoustic emission

ABSTRACT

Mechanics of double-lap Steel-to-CFRP adhesively-bonded joints loaded in tension are investigated experimentally using Digital Image Correlation (DIC) and Acoustic Emission (AE), analytically using a one-dimensional closed-form solution and numerically with Finite Element analysis. The double-lap bi-material joints are fabricated of a steel core adhesively bonded to two CFRP skins with adhesive thickness of ~ 8 mm, using an Epoxy-based and MMA-based adhesives. In order to capture the in-plane deformation of the joint, full field strain/displacement maps are obtained using DIC. This data is used to validate the shear-lag model predictions of the adhesive shear stress/strain distribution as well as the linear-elastic Finite Element Model (FEM) results. In addition, they are used to capture the susceptible damage locations and their effect on the displacement contour maps, strain distribution and load transfer between the joint's different constituents. A correlation between the DIC displacement and the AE signals is obtained for damage detection in both joints. Moreover, a good agreement amongst the analytical, FE and DIC strain/stress distributions along the bond-line is observed. This study introduces the analytical shear-lag model as an alternative to predict the stress state in thick-adhesive double-lap joints, with an acceptable level of accuracy and robustness.

1. Introduction

The use of adhesively-bonded double-lap joints (DLJs) is preferred over conventional joining techniques such as bolting, riveting and welding. They offer many advantages including, for instance, the ability to join dissimilar materials such as steel and fiber reinforced composites, weight savings, improved stress distribution along the bond-line and enhancement of the corrosion and fatigue resistance characteristics [1–3]. Such characteristics are essential, especially in maritime applications. However, the dominant damage mechanisms in these joints may vary based on various factors including: loading conditions, environmental conditions, mechanical properties of adhesive and adherends, adhesive thickness and also the adhesion quality between the adhesive and adherends. These damage mechanisms include, but are not limited to: interfacial failure between the adherends and adhesive layer (i.e., adhesive failure), cohesive failure within the adhesive layer and failure within the adherends [4,5]. Therefore, a deep and thorough understanding of the mechanics of the bi-material adhesively-bonded joints is essential to fully utilize their capabilities in industrial applications. Experimentally, various techniques have been employed to study the stresses and damage evolution in adhesively bonded joints including, but not limited to, Digital Image Correlation (DIC) [6–8] and Acoustic Emission (AE) [9–11]. Thäsler et al. [6] proposed a method to measure and track the crack growth in fatigue-loaded adhesively bonded CFRP joints using DIC. They applied their technique to single and double-lap shear adhesively-bonded joints. Moreover, Saeedifar et al. [7] characterized the damage in bi-material steel-to-composite double-lap adhesively-bonded joints using the combination of AE and supervised clustering techniques. In addition, they successfully validated the classified damage mechanisms against DIC, Fiber Optic Sensor (FOS) and camera results.

Beside experimental techniques, to understand the mechanics and stress state in DLJ, analytical approaches can represent an alternative to numerical modelling providing closed-form solutions with an acceptable level of accuracy and robustness. Comprehensive literature reviews [12–14] are available detailing the performance of various analytical models in predicting the stress distribution for both single and double-lap joints for similar and dissimilar adherends. Da Silva et al. [12] concluded that almost all the available analytical models are two-dimensional, which is sufficient as the stresses in the width direction are generally lower than the loading direction. In addition, most of the models are limited to the linear-elastic regime for both the adherends and the adhesive as non-linearity introduction leads to very complex solutions which might require to be solved numerically at the end.

* Corresponding author.
E-mail address: m.a.s.n.saleh@tudelft.nl (M.N. Saleh).

https://doi.org/10.1016/j.ijadhadh.2019.102480

Available online 5 November 2019

They also discussed the limitations of the classical analytical models which include: i) neglecting the adherends' shear deformation, ii) assuming only linear adhesive response and iii) overestimating the stress at the end of the overlap by violating the stress-free condition. This overestimation results in a conservative failure load prediction when designing DLJs. As an attempt to overcome these limitations, the improved shear-lag model, by Tsai et al. [15] for double-lap adhesively-bonded joints, was proposed to take into account the shear deformation in the adherends. Moreover, Liu et al. [16] introduced a closed-form solution to the stress/strain distribution in bi-material bonded joints using ductile adhesive. In their model, they accounted for the adhesive plasticity. Again based on a shear-lag formulation which was validated against experimental results, the model was able to analyze an arbitrary thermal and mechanical loading condition. Moreover, Shishesaz et al. [17] investigated the effect of adhesive thickness and viscoelasticity on the shear stress distribution in DLJs using analytical models. Results reported a drop in the peak shear stress to almost 1/3 of its initial value by increasing the thickness from 0.01 to 0.1 mm. In addition, a defined ratio of the viscous effect to the shear modulus of the adhesive is found to have an adverse effect on the peak shear stress in the joint. Although this study investigated the adhesive thickness effect, still the maximum thickness investigated (~0.1 mm) is considered very thin for applications such as maritime applications, which is the focus of the current study.

To the authors' knowledge, there is almost no study in the literature investigating the potential of using shear-lag analytical approaches for relatively thick (~8 mm) adhesively-bonded bi-material DLJs. Thus, the objective, of this study, is to determine to what extent analytical models "such as the improved Tsai model" can be reliable in predicting and understanding the stress state in bi-material thick adhesively-bonded joints in the light of using DIC and Finite Element (FE) models. Two different structural adhesives, representing a ductile (Methacrylate-based) and brittle (Epoxy-based) types, are used to bond CFRP skins to a steel core. The fabricated joints are loaded in tension while damage evolution is monitored by DIC and AE. Results from the DIC displacement/strain map are used to validate the distributions obtained from the analytical Tsai-improved model and a linear-elastic FE model. Besides, the damage and failure analysis is studied by correlating the AE cumulative energy with the macroscopic load-displacement of the DLJ and the DIC displacement distributions at specific locations. Finally, a summary of the concluding remarks of this research study is provided.

2. Materials and manufacturing

2.1. Adherends and adhesives

The steel used in this study is high strength structural shipbuilding steel AH36 with Young's modulus of ~ 200 GPa, yield strength of 350 MPa, ultimate strength of (400–550) MPa and Poisson's ratio of 0.26. The CFRP laminates are produced using vacuum infusion. In order to avoid galvanic corrosion, a thin layer of chopped-glass fiber fabric was used on both sides. The lay-up was quasi-isotropic, with the 0°-direction in the length direction of the final specimen geometry. The thickness of the steel plate and the CFRP laminate used is 8 mm and 2.5 mm respectively. The first adhesive used to bond the steel and CFRP adherends is a two-component toughened epoxy adhesive with a mixing ratio of 2:1 by volume. The adhesive tensile modulus is ~ 2 GPa with a tensile strength of ~ 35 MPa and strain to failure of 10% as per the manufacturer datasheet. The second adhesive used is a two-component Methacrylate adhesive with a mixing ratio of 10:1 by volume. The adhesive tensile modulus is ~200 MPa with a tensile strength of ~ 15 MPa and strain to failure of 40–60% as per the manufacturer datasheet.

2.2. Joint design and manufacturing

The DLJ specimen consists of two steel cores separated by a gap

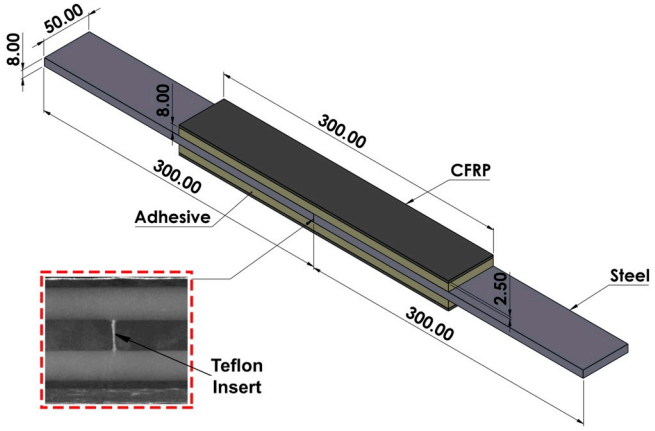

Fig. 1. Schematic of the DLJ specimen (dimensions in mm).

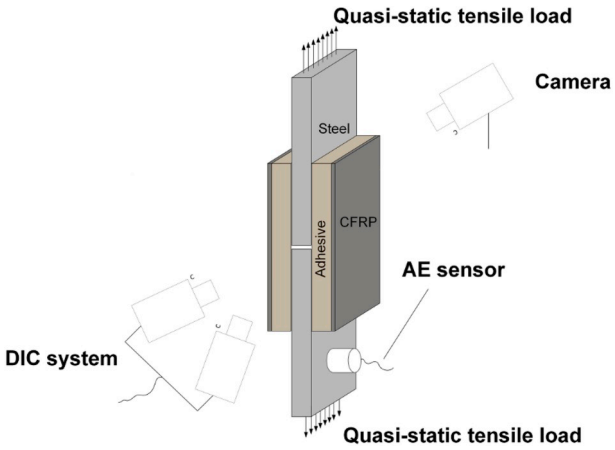

Fig. 2. Schematic of the DLJ test setup.

"Teflon insert" and bonded with thick adhesive layers (~8 mm) to CFRP skins as depicted in Fig. 1. The shop primer on the steel was removed by grit blasting up to SA2.5. Then, the adherends' surfaces were cleaned and degreased with isopropanol prior to bonding.

3. Experimental procedure

3.1. Test setup

The test setup schematic depicted in Fig. 2 consists of four main data acquisition systems. The Universal Testing Machine (UTM) records the load and the cross-head displacement. The corresponding displacement and the strain contour measurements are acquired by processing in-situ images captured by a 3D DIC system from one side. A camera continuously monitors the cross-section of the specimen during the loading process from the opposite side. And one Acoustic Emission (AE) sensor is placed on the lower steel adherend to capture the AE signals generated during the test. Tensile testing was conducted as per the guidelines of ASTM D3528 standard for "Strength Properties of Double-lap Shear Adhesive Joints by Tension Loading" [18]. Universal Testing Machine (Zwick Roell) with 250 kN load cell is used to apply a displacement controlled tension with a rate of 1.27 mm/min according to the standard. Three specimens are tested for each adhesive type.

3.2. Digital Image Correlation (DIC)

The DIC system used for the full-field strain measurement consists of two 8-bit "Point Grey" cameras with "XENOPLAN 1.4/23" lenses. Both

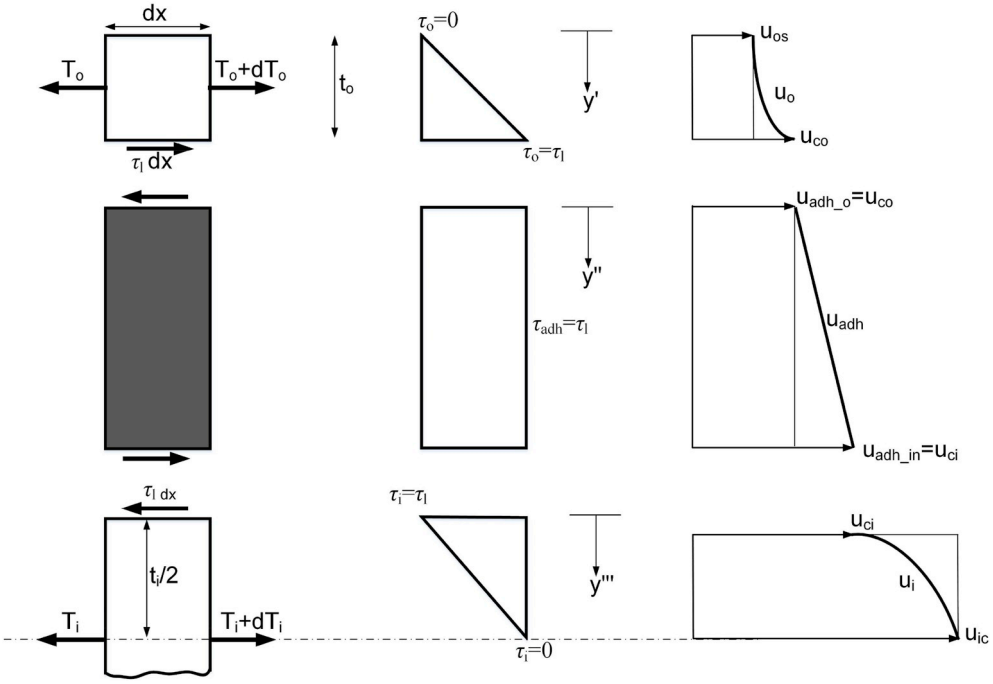

Fig. 3. Analytical model's assumptions for the displacement and shear stress distribution across the thickness of the adherends and the adhesive.

cameras have a resolution of 5 MP. Vic-Snap 8 software was used to record the speckle pattern images from the cameras, and the 3D DIC system was calibrated before the testing. The acquisition frame rate was set to 3 frames per second (fps) for the uniaxial tensile testing. The speckle pattern images acquired by Vic-Snap 8 were then processed using Vic-3D 8 software. In processing these images, the subset size was set to 21 × 21 pixels with a step size (distance between subsets) of 7 pixels. The observation window of approximately (600 × 30) mm^2 produced an image with dimensions of (2048 × 102) pixels. Global mean values of strains (ε_{xx};ε_{yy};ε_{xy}) are obtained from DIC analysis using Vic-3D 8 software.

3.3. Acoustic emission (AE)

One AE sensor was mounted on the steel, and the AE signals recorded were used for all the analysis. The AE sensor was a broadband, resonant-type, and single-crystal piezoelectric transducer from Vallen Systeme GmbH, AE1045S-VS900 M, with external 34 dB preamplifier and an operating frequency range of [100–900 kHz]. To eliminate the surrounding noises, the threshold was set to 50 dB. An AMSY-6 Vallen, 8-channel acoustic emission system with the sampling rate of 2 MHz, was used to record the AE signals. Ultrasound gel was applied between the surfaces of the sensor and the specimen to ensure good acoustical coupling. A standard pencil lead break procedure [19] was used to check the connection between the specimen and the AE sensor surface prior to the mechanical test.

4. Theory and modelling

4.1. One-dimensional shear-lag model

The classical solution for stress analysis in single-/double-lap joints was first proposed by Volkersen and Bruyne [20]. It is a shear-lag approach modelling the adherends, without considering their shear deformation, as bars, while the adhesive is considered as a shear spring transferring the longitudinal forces from the inner to the outer adherend via shear loading only. Nevertheless, the improved shear-lag based model, proposed by Tsai et al. [15] for double-lap adhesively-bonded joints, takes into account the shear deformation in the adherends. The main assumptions for this model is the linear shear stress across the thickness of the adherends with a traction-free surface of the outer adherend and zero shear stress in the middle of the inner adherend. Originally, the Tsai improved model was proposed for thin adhesive bond-lines [15,21]. The major difference in this study is utilizing the Tsai model for thick adhesive layers (~8 mm) rather than using it for thin adhesive cases like in the literature. The model assumptions are still valid because the shear stress is assumed to be constant throughout the adhesive thickness. This assumption can be justified due to the fact that the shear modulus of the adhesive layer is very small compared to the "stiff" adherends, and it will be further confirmed using the numerical (FEM) analysis (see Section 5.2.1). Similar to the original proposed model, the shear stress/strain is assumed to be linear across the thickness of the adherends, which are the CFRP (outer adherend) and steel (inner adherend) in this case, as depicted in Fig. 3. Due to symmetry, the mid-plane of the steel (inner adherend) has zero shear stress. The outer surfaces of the outer adherends are stress free ($\tau_o = 0$). The displacement distribution across the joint thickness is highlighted in Fig. 3.

The total overlap length is 2l. The thickness of the inner and outer adherends are t_i and t_o, respectively. The elastic modulus of the outer adherend is denoted as E_o, while the shear modulus is denoted as G_o. The same applies for the inner adherend with changing the subscript as E_i and G_i for the elastic modulus and shear modulus. For the adhesive layer, the shear modulus is denoted as G_a with a thickness of t_a.

The applied load per unit width is denoted as T resulting in an average shear stress (τ_{avg}) along the bond-line:

$$\tau_{avg} = \frac{1}{2l}\int_{-l}^{l} \tau_l dx = \frac{T}{4l} \tag{1}$$

where τ_l is the adhesive shear stress governed by the equation:

$$\frac{d^2\tau_l}{dx^2} - \beta^2\tau_l = 0 \tag{2}$$

which leads to the closed form solution of τ_l. The reader is referred to Ref. [15] for the detailed derivation of the model.

$$\tau_l = A\sinh(\beta x) + B\cosh(\beta x) \tag{3}$$

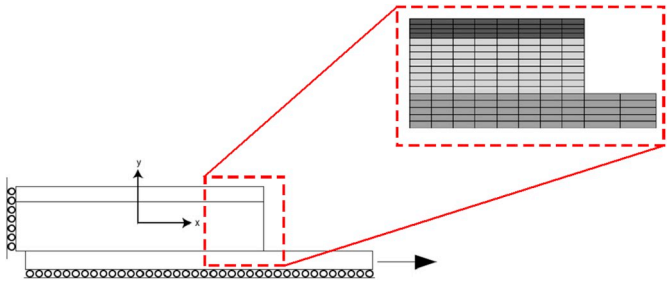

Fig. 4. Schematic of the FEM boundary conditions and the applied mesh.

Table 1
Summary of material and geometrical parameters for the adherends and the adhesives.

Parameter	Outer adherend	Adhesive		Inner adherend
Material	CFRP*	Epoxy	MMA	Steel
Thickness (mm)	2.50	8.00	8.00	8.00
Tensile modulus (GPa)	37.43 ± 1.14	2.00	0.20	200
Poisson's ratio	0.32 ± 0.01	0.30	0.30	0.26
Shear modulus (GPa)	13.78 ± 0.25	0.77	0.08	79.37

* Tested experimentally.

A and B are constants determined from the boundary conditions at the edges of the bond-line (Eqn. (2)):

$$T_o = \frac{T}{2} = 2l\tau_{avg}, \quad T_i = 0 \qquad \text{at} \quad x = -l \tag{4a}$$

$$T_o = 0, \quad T_i = T = 4l\tau_{avg} \qquad \text{at} \quad x = l \tag{4b}$$

resulting in:

$$A = \frac{\beta l \tau_{avg}}{\cosh(\beta l)} \left[\frac{1 - \frac{E_i t_i}{2E_o t_o}}{1 + \frac{E_i t_i}{2E_o t_o}} \right] \tag{5}$$

$$B = \frac{\beta l \tau_{avg}}{\sinh(\beta l)} \tag{6}$$

In addition, the parameter β can be described by two components: λ (an elongation component) and α (a shear deformation component).

$$\beta^2 = \alpha^2 \lambda^2 \tag{7}$$

$$\lambda^2 = \frac{G_a}{t_a}\left(\frac{2}{E_i t_i} + \frac{1}{E_o t_o}\right) \tag{8}$$

$$\alpha^2 = \left[1 + \frac{G_a}{t_a}\left(\frac{t_i}{6G_i} + \frac{t_o}{3G_o}\right)\right]^{-1} \tag{9}$$

4.2. Numerical (FE) analysis

To further investigate the mechanics of the DLJs, a 2D linear elastic FE model is implemented using ABAQUS Standard. Dimensions of the actual tested specimen, detailed in section 2.2, are used as an input for the model geometry. Due to two planes of symmetry, only a quarter of the joint is modeled (see Fig. 4). Roller boundary conditions replacing the planes of symmetry are defined while the gap edge is defined as a free surface. The load is applied as a constant displacement boundary condition along the steel "inner adherend" edge.

A zoomed-in picture is highlighted to show the mesh density used in this study. In addition, a plane strain condition was used for the simulation while specifying the width in the elements definition. In this case, the three-dimensional free-edge effect [22] is neglected. The element type used was CPE4R, a linear quadrilateral reduced integration element. The total number of elements was 1840 elements. Besides, The materials' mechanical properties are detailed in Table 1.

5. Results and discussion

5.1. Load-displacement curves

The load-displacement curves of the DLJ specimens are depicted in Fig. 5. The load-displacement response of the Epoxy-based specimens is almost linear up to the final failure, which can be described as a brittle fracture. On the contrary, the load-displacement response for the MMA-based specimens has a nonlinear behavior from the beginning of the test up to the final failure with a significant plasticity and damage progression leading to a ductile fracture. It is clear from the load-displacement data that there is a trade-off between the strength and the ductility "strain to failure" of the adhesives. In the case of the MMA adhesive, the displacement to failure is approximately 4 times higher than the Epoxy-based; while the strength of the Epoxy is almost 1.6 times higher than the MMA-based counterpart.

5.2. Analytical and numerical analysis

5.2.1. Through the thickness

Using the FEM model, the shear stress distribution through the thickness of the double-lap joint is determined for both adhesive types as depicted in Fig. 6. The shear stress distribution across the thickness confirms the assumptions made earlier for the derivation of the analytical model. The shear stress is linear in the outer adherend "CFRP" and the inner adherend "steel", with the mid-plane experiencing zero

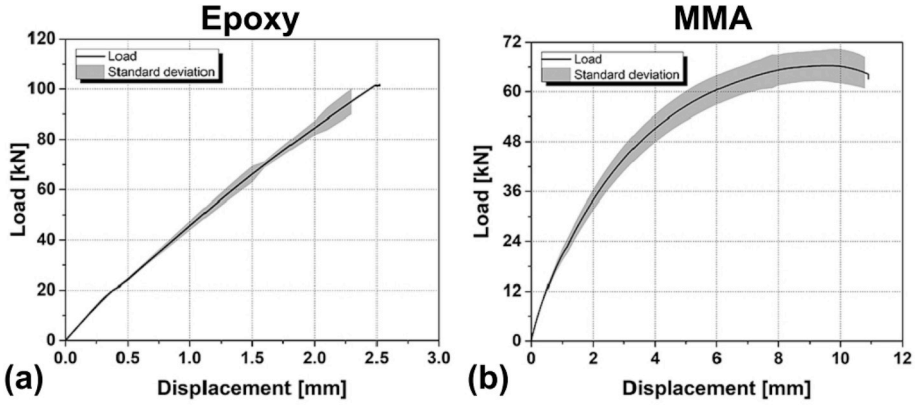

Fig. 5. Load-displacement curves of the DLJs for: a) the Epoxy-based and b) the MMA-based adhesives.

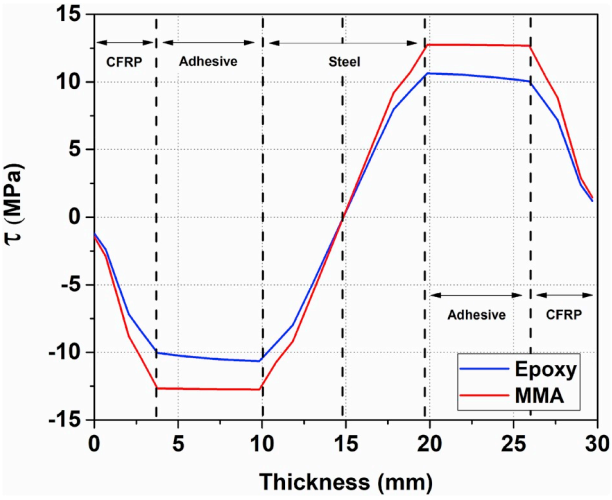

Fig. 6. The shear stress distribution, across the thickness of the DLJ specimen, using the FE linear elastic model.

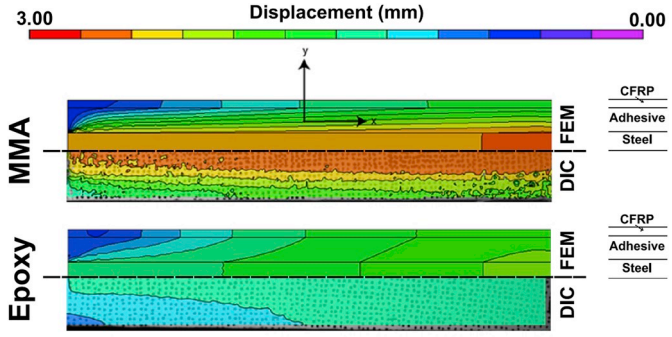

Fig. 7. Comparison between the experimental (DIC) displacement and the predicted (FEM) displacement fields.

shear stress. In addition, the stress is almost constant in both adhesives, especially the MMA based. This confirms the assumption made to derive the equations for the analytical model.

The displacement contour map, obtained from the DIC analysis during the experimental testing, is compared against the FEM predicted displacement map in Fig. 7. For both adhesives, there is a good agreement between the DIC and FEM displacement distribution across the thickness of the joints. Moreover, the gradient of displacement in the MMA-based adhesive is found to be much larger than the Epoxy-based case. Due to the ductile nature of the MMA-based adhesive, it experiences larger deformation (see Fig. 7). This directly results in higher shear strain imposed/transferred via the MMA-based adhesive for the same applied deformation "displacement".

5.2.2. Along the bond-line

A schematic of half of the DLJ is depicted in Fig. 8 to use as a reference for the discussion in this section. The comparison of the DIC experimental, Tsai analytical and FE numerical results is depicted in Fig. 8a. The normalized shear strain/stress is defined as the shear strain divided by the average shear strain at the same load/displacement. In the case of similar adherends, the distribution of normalized shear strain/stress is reported to be symmetric along the bond-line [15,17,21,23]. However, in the case of dissimilar adherends, this symmetry vanishes (see Fig. 8a). There is a clear shift of the minimum stress away from the gap "Teflon insert". Although the Tsai closed-form solution was introduced in literature for thin adhesive bond-lines, the use of it for thick adhesive layers seems to be valid, with the assumption of constant shear stress across its thickness. In general, the predictions from the Tsai model and FE model are off, at the gap's vicinity, which can be attributed to the stress singularity at this location ($x/l < -0.5$). For both adhesive types, the Tsai analytical model and the FE model predict the normalized strain/stress distribution along the bond-line with a good level of accuracy, especially away from the gap ($x/l > -0.5$).

The FEM predicted adhesive shear (τ) and peel (σ) stresses, normalized by the average shear stress in the adhesive (τ_{avg}), are shown in Fig. 8b. The peel stress is defined as the transverse normal stress experienced by the joint due to the global applied tensile loading. It is an important stress component to consider as it might result in the initiation of the joint's failure. It is clear from the results of the two adhesive

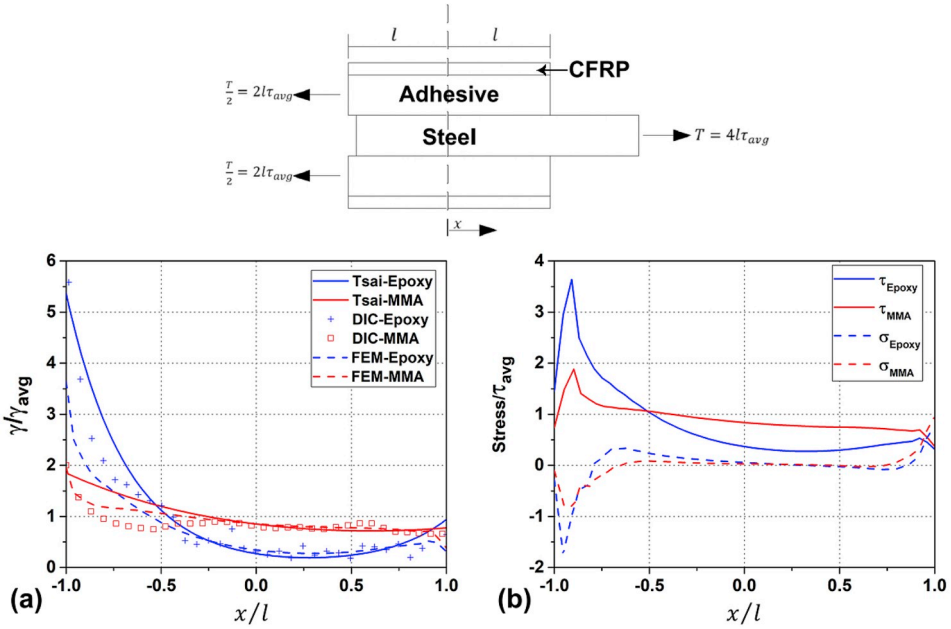

Fig. 8. Comparison of the normalized: a) shear stress/strain from DIC, Tsai and FEM and b) shear and peel stress from FEM, along the bond-line for both adhesive joints.

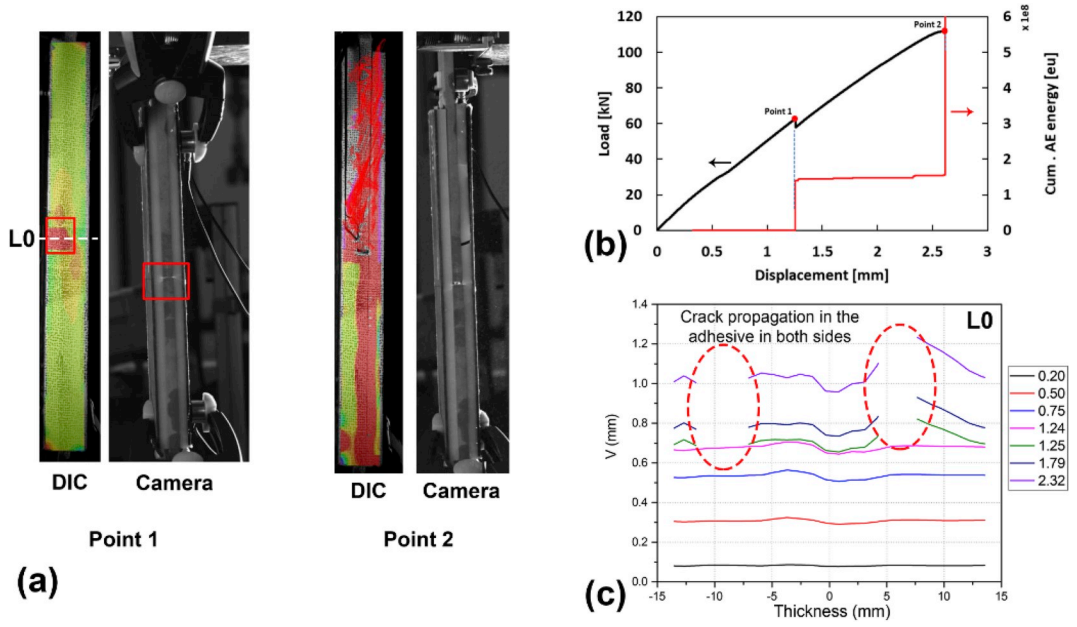

Fig. 9. Damage evolution for Epoxy-based DLJ: a) DIC and camera, b) Load-displacement correlation with the cumulative AE energy and c) Vertical Displacement along L0.

types that the maximum stresses are located at the center of the joint where the initial gap is. When it comes to comparing the normalized shear stress between the two adhesive types, the maximum values are captured at the center of the joint ($x/l = -1$). In this case, the Epoxy-based adhesive experiences higher shear stress in the vicinity of the gap. However moving away from the gap in the center, the shear stress for the Epoxy-based is lower than the MMA-based counterpart. It is also clear from the comparison between the two adhesive types that unlike the shear stress, the peel stress distribution along the bond-line is not affected by the adhesive type. Only very close to the center of the joint ($x/l = -1$) at the end of the overlap, the compressive peel stress in the Epoxy-based is almost double the peel stress in the MMA-based adhesive. This confirms the conclusions from previous studies [24,25] recommending the use of flexible/ductile adhesive to reduce the peel stresses at the end of the overlap. Although the DLJs are designed to reduce the peel stresses as opposed to the single-lap joints [25], the peel stresses can still lead to the joint failure and the reduction of the joint shear capacity to transfer the load from the inner to the outer adherend via the adhesive. The induced peel stresses due to the joint's loading condition results in a moment at the end of the overlap which might lead to the failure initiation of the joint. This effect is more significant when one of the adherends is FRP composites because their transverse (through the thickness) poor mechanical properties can represent the weakest point of the joint [11,26]. The composite adherend probably

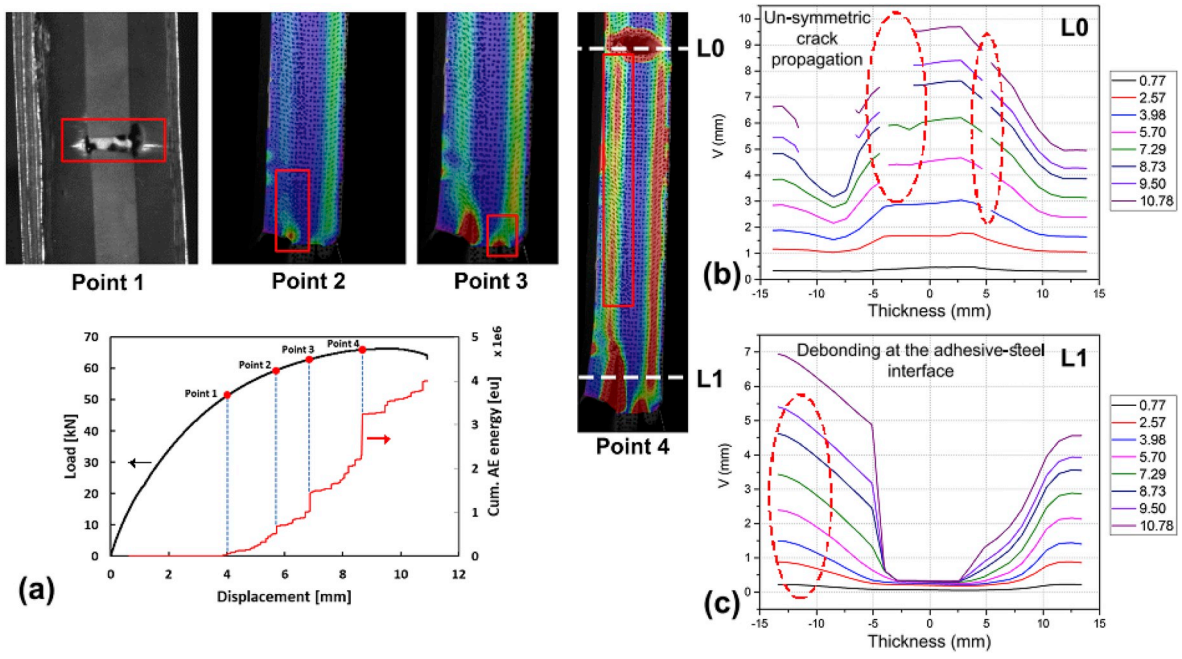

Fig. 10. Damage evolution for MMA-based DLJ: a) DIC and camera and the load-displacement correlation with the cumulative AE energy, b) Vertical Displacement along L0 and c) Vertical Displacement along L1.

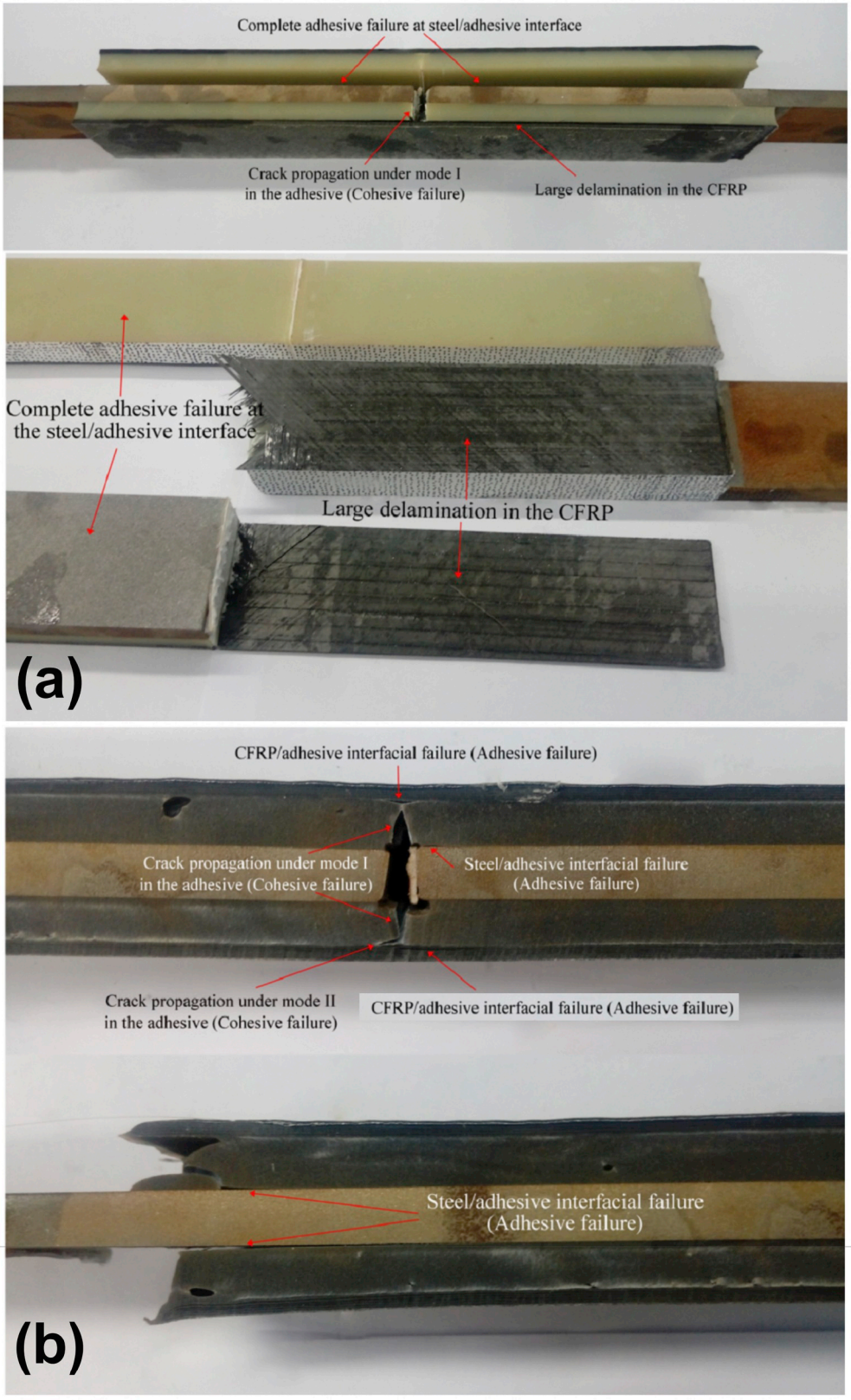

Fig. 11. Damage mechanisms observed in the fractured DLJ specimens: a) Epoxy-based and b) MMA-based.

fails in transverse tension prematurely even before the adhesive fails. Thus, it is essential to fully understand its distribution along the bond-line and try to optimize the joint design accordingly.

5.3. *Damage and failure analysis*

The AE signals captured during the tensile testing of the DLJs, for both adhesive types, are correlated with the DIC displacement maps and

the camera images to confirm the different damage events. Fig. 9 demonstrates the load-displacement curve for the Epoxy-based DLJ as well as the cumulative AE energy. The cumulative AE energy is calculated as the summation of the energies of the individual AE signals captured during the test. As expected from the brittle nature of the adhesive, the stiffness of the joint is almost linear with a sudden drop of the load (see point 1 in Fig. 9b) at approximately 1.25 mm then linear again up till failure (see point 2 in Fig. 9b). The same pattern is confirmed from the cumulative AE energy curve as point 1 shows a sudden increase in the cumulative energy indicating strain energy released due to a damage event. From the DIC displacement/strain map and the line plot of the displacement in the center of the joint at the gap "Teflon insert" position, a clear discontinuity in the displacement is observed (see Fig. 9c). This discontinuity corresponds to the crack propagation in the thick adhesive layer leading to the strain concentration in the DIC map (see Fig. 9a). The second sudden increase in the Cumulative AE energy curve occurs instantaneously at the final failure. This increase is significantly larger than the first one as it corresponds to the rupture of the joint at multiple locations. The DIC and camera images clearly indicate the multiple fractures in the adhesive layer as well as debonding at the steel/adhesive interface "adhesive failure" and delamination in the CFRP skin.

Unlike the Epoxy-based adhesive, the MMA-based DLJ demonstrates a non-linear load-displacement response with cumulative AE energy increase at different displacements, as shown in Fig. 10a. The exact same approach used to understand the source of these increases, combining the input from the DIC strain/displacement maps and the camera images, is utilized. Four main points on the load-displacement, based on the cumulative AE energy curves, are identified. The initiation of the crack in the adhesive layer (at point 1 in Fig. 10a) results in energy dissipation captured by the AE system and a discontinuity in the DIC displacement map (see line plot in Fig. 10b and DIC map at point 1). Then, at higher loading levels (Points 2 and 3), the crack in the middle of the joint continues growing (see Fig. 10b) in addition to steel/adhesive debonding "adhesive failure" occurring at the lower edge of the DLJ (see Fig. 10c). Finally towards the end of the test, the debonding at the steel/adhesive interface from the center of the DLJ and the lower edge join (see point 4 in Fig. 10a) leading to the largest increase in the cumulative AE energy at point 4. These observations are supported by the DIC strain map in Fig. 10a–c.

Fig. 11 demonstrates the post mortem fractured DLJs for the two types of specimens investigated in this study. From the visual inspection, it is clear that different damage mechanisms can be spotted for the two adhesive types. In the case of the Epoxy-based adhesive joint (see Fig. 11a), a transverse crack extending from the gap leads to a cohesive failure in the adhesive under mode I. On the other side of the joint, a complete adhesive failure occurs at the steel/adhesive interface. Moreover, interlaminar delamination in the CFRP skin is obvious. For the MMA-based adhesive joint (see Fig. 11b), again crack propagation "cohesive failure" from the gap under mode I is observed. At the crack tip singularity, local adhesive failure occurs at the CFRP/adhesive interface. In addition, some adhesive failure at the steel/adhesive interface can be spotted in the center of the specimen at the vicinity of the gap. Larger adhesive failure at the steel/adhesive interface occurs at the free edges of the joint. However, there are no signs of any interlaminar delamination in the CFRP skin in this case.

6. Conclusion

The mechanics and stresses of double-lap Steel-to-CFRP adhesively-bonded joints, with thick adhesive layer, loaded in tension were investigated experimentally using Digital Image Correlation (DIC) and Acoustic Emission (AE), analytically using a one-dimensional closed-form solution and numerically with Finite Element analysis. The double-lap bi-material joints were fabricated of a steel core adhesively bonded to two CFRP skins with adhesive thickness of ~ 8 mm, using an Epoxy-based and MMA-based adhesives. From the analysis performed, the following conclusions can be drawn:

- The improved Tsai analytical model, used for thick adhesive layers and assuming a constant shear stress through the thickness, proved to yield an acceptable level of accuracy to predict the stress state in thick-adhesive bi-material DLJs.
- Unlike similar adherends DLJs, it was observed that the stress distribution symmetry along the bond-line vanishes for dissimilar adherends. Moreover, the peel stresses distribution predicted by the FEM suggested that highest peel stress occurs at the vicinity of the gap in the center of the DLJ
- The gradient of displacement in the MMA-based adhesive, through the joint thickness obtained from FEM and DIC, is found to be larger than the Epoxy-based case. This is due to the ductile nature of the adhesive as opposed to the Epoxy-based counterpart.
- AE cumulative energy and DIC displacement maps successfully identified the damage evolution for DLJs during testing.

Acknowledgments

This research was carried out within the project "QUALIFY–Enabling Qualification of Hybrid Joints for Lightweight and Safe Maritime Transport (2S03-051)", co-funded by the INTERREG 2Seas Mers Zeeën programme.

References

[1] Sousa JM, Correia JR, Firmo JP, Cabral-Fonseca S, Gonilha J. Effects of thermal cycles on adhesively bonded joints between pultruded GFRP adherends. Compos Struct 2018;202:518–29. https://doi.org/10.1016/j.compstruct.2018.02.081.
[2] Mariam M, Afendi M, Abdul Majid MS, Ridzuan MJM, Azmi AI, Sultan MTH. Influence of hydrothermal ageing on the mechanical properties of an adhesively bonded joint with different adherends. Compos B Eng 2019;165:572–85. https://doi.org/10.1016/j.compositesb.2019.02.032.
[3] Yang Y, Biscaia H, Chastre C, Silva MAG. Bond characteristics of CFRP-to-steel joints. J Constr Steel Res 2017;138:401–19. https://doi.org/10.1016/j.jcsr.2017.08.001.
[4] Heshmati M, Haghani R, Al-Emrani M. Durability of bonded FRP-to-steel joints Effects of moisture, de-icing salt solution, temperature and FRP type. Compos B Eng 2017;119:153–67. https://doi.org/10.1016/j.compositesb.2017.03.049.
[5] Heshmati M, Haghani R, Al-Emrani M, André A. On the strength prediction of adhesively bonded FRP-steel joints using cohesive zone modelling. Theor Appl Fract Mech 2018;93:64–78. https://doi.org/10.1016/j.tafmec.2017.06.022.
[6] Thäsler T, Holtmannspötter J, Gudladt HJ. Monitoring the fatigue crack growth behavior of composite joints using in situ 2D-digital image correlation. J Adhes 2019;95:595–613. https://doi.org/10.1080/00218464.2018.1562923.
[7] Saeedifar M, Saleh MN, De Freitas ST, Zarouchas D. Damage characterization of adhesively-bonded Bi-material joints using acoustic emission. Compos B Eng 2019;176. https://doi.org/10.1016/j.compositesb.2019.107356.
[8] Katnam KB, Dhôte JX, Young TM. Experimental analysis of the bondline stress concentrations to characterize the influence of adhesive ductility on the composite single lap joint strength. J Adhes 2013;89:486–506. https://doi.org/10.1080/00218464.2013.759432.
[9] Fotouhi M, Saeedifar M, Sadeghi S, Najafabadi MA, Minak G. Investigation of the damage mechanisms for mode I delamination growth in foam core sandwich composites using acoustic emission. Struct Health Monit 2015;14:265–80. https://doi.org/10.1177/1475921714568403.
[10] Xu D, Liu PF, Li JG, Chen ZP. Damage mode identification of adhesive composite joints under hygrothermal environment using acoustic emission and machine learning. Compos Struct 2019;211:351–63. https://doi.org/10.1016/j.compstruct.2018.12.051.
[11] Kupski J, Teixeira de Freitas S, Zarouchas D, Camanho PP, Benedictus R. Composite layup effect on the failure mechanism of single lap bonded joints. Compos Struct 2019;217:14–26. https://doi.org/10.1016/j.compstruct.2019.02.093.
[12] da Silva LFM, das Neves PJC, Adams RD, Spelt JK. Analytical models of adhesively bonded joints-Part I: literature survey. Int J Adhesion Adhes 2009;29:319–30. https://doi.org/10.1016/j.ijadhadh.2008.06.005.
[13] Baldan A. Review. Adhesively-bonded joints in metallic alloys, polymers and composite materials: mechanical. J Mater Sci 2004;39:4729–97.
[14] da Silva LFM, das Neves PJC, Adams RD, Wang A, Spelt JK. Analytical models of adhesively bonded joints-Part II: comparative study. Int J Adhesion Adhes 2009;29:331–41. https://doi.org/10.1016/j.ijadhadh.2008.06.007.
[15] Tsai MY, Oplinger DW, Morton J. Improved theoretical solutions for adhesive lap joints. Int J Solids Struct 1998;35:1163–85. https://doi.org/10.1016/S0020-7683(97)00097-8.

[16] Liu M, Dawood M. A closed-form solution of the interfacial stresses and strains in steel beams strengthened with externally bonded plates using ductile adhesives. Eng Struct 2018;154:66–77. https://doi.org/10.1016/j.engstruct.2017.10.054.
[17] Shishesaz M, Reza A. The effect of viscoelasticity of adhesives on shear stress distribution in a double-lap joint using analytical method. J Adhes Sci Technol 2013;27:2233–50. https://doi.org/10.1080/01694243.2013.769085.
[18] ASTM D3528. Standard test method for strength properties of double lap shear adhesive joints by tensile loading, i; 2012. p. 1–4. https://doi.org/10.1520/D3528-96R08.2.
[19] ASTM E976. Standard guide for determining the reproducibility of acoustic emission sensor response. Astm 2015:1–7. https://doi.org/10.1520/E0976-15.2.
[20] Bruyne BNA De. Workshop and production section the strength of glued joints. Aircr Eng 1944;115–8.
[21] Tsai MY, Morton J. An investigation into the stresses in double-lap adhesive joints with laminated composite adherends. Int J Solids Struct 2010;47:3317–25. https://doi.org/10.1016/j.ijsolstr.2010.08.011.
[22] Tsai MY, Morton J, Matthews FL. Experimental and numerical studies of a laminated composite single-lap adhesive joint. J Compos Mater 1995;29:1254–75. https://doi.org/10.1177/002199839502900906.
[23] CHEN D, MASUDA K. Analysis of stresses in double-lap. Trans JAPAN Soc Mech Eng Ser A 2013;79:49–59. https://doi.org/10.1299/kikaia.79.49.
[24] das Neves PJC, da Silva LFM, Adams RD. Analysis of mixed adhesive bonded joints Part II: parametric study. J Adhes Sci Technol 2009;23:35–61. https://doi.org/10.1163/156856108X336035.
[25] Banea MD, Da Silva LFM. Adhesively bonded joints in composite materials: an overview. Proc Inst Mech Eng L J Mater Des Appl 2009;223:1–18. https://doi.org/10.1243/14644207JMDA219.
[26] da Silva LFM, Adams RD. Techniques to reduce the peel stresses in adhesive joints with composites. Int J Adhesion Adhes 2007;27:227–35. https://doi.org/10.1016/j.ijadhadh.2006.04.001.